Director reorientation in a hybrid-oriented liquid-crystal film induced by thermomechanical effect

A. V. Zakharov* and A. A. Vakulenko†

Saint Petersburg Institute for Machine Sciences, The Russian Academy of Sciences, Saint Petersburg 199178, Russia

(Received 22 April 2009; published 24 September 2009)

We have carried out a numerical study of a system of hydrodynamic equations including director reorientation, fluid flow, and temperature redistribution across a two-dimensional (2D) hybrid-oriented liquid-crystal (HOLC) cell under the influence of a heat flow directed normal to the upper bounding surface, whereas on the rest boundaries the temperature is kept constant. Calculations based upon the nonlinear extension of the classical Ericksen-Leslie theory shows that the HOLC material under the influence of the heat flow, after some time, more than the time of relaxation, for instance, of the director field in the HOLC cell, settles down to the rest state regime, where the horizontal and vertical components of the velocity vector are equal to zero, and the temperature field across the LC cell finally reaches the value of temperature on the lower and two lateral bounding surfaces. The role of hydrodynamic flow in the relaxation processes of the temperature field to its equilibrium distribution across the 2D HOLC cell, containing 4−n−pentyl−4′−cyanobiphenyl, has been investigated, for a number of dynamic regimes.

DOI: 10.1103/PhysRevE.80.031711 PACS number(s): 61.30.−v, 47.57.Lj, 65.40.De

I. INTRODUCTION

The widely used flat-panel liquid-crystal displays (LCDs) consist of a liquid-crystal (LC) film sandwiched between two glass or plastic surfaces on the scale of the order of micrometers across which a voltage may be applied, independently to each pixel of the LCD. In this structure, the transmission of light through individual pixels is controlled by a potential difference applied between electrodes on the back plate of the LCD [1]. This applied electric field may alter the molecular configuration of the LC layer and thus alter the optical characteristics of the LCD. In the field of LC phases, a great deal is known about their deformations under the influence of electric or magnetic fields [2], whereas, on the other hand, comparatively little is known about the effect of temperature gradient on their structure properties [3–8].

The purpose of this paper is to show, in the framework of the nonlinear extension of the Ericksen-Leslie theory [9,10], together with accounting for the thermoconductivity equation for the temperature field $T(t,\mathbf{r})$ [11], the way how in the microscopic scale two-dimensional (2D) hybrid-oriented LC (HOLC) cell can dissipate the energy which has been injected into the LC cell, for instance, across the upper restricted surface. The second aim is to show how much influences both the direction and magnitude of the hydrodynamic flow $\mathbf{v}$ produced by induced heating on the director reorientation $\hat{\mathbf{n}}(t,\mathbf{r})$ across the HOLC cell.

Understanding how an elastic soft material, such as LCs, deforms under the influence of external forces, both temperature gradient and mechanical efforts, is a question of great fundamental interest, as well as an essential piece of knowledge in material science. Despite the fact that certain qualitative and quantitative advances in a hydrodynamic description of the relaxation processes in the LC phase under the influence of temperature gradient have been achieved, it is still too early to talk about the development of a theory which would make it possible to describe the dissipation processes in confined LC phase. But taking into account that the demand for increased resolution grows, along with miniaturization for projected-based LCDs, such advances are a question of great technological interest too [12].

The outline of this paper is as follows. The system of hydrodynamic equations describing both director motion and fluid flow of a liquid-crystal phase confined between two horizontal and two lateral bounding surfaces, with accounting for the heat flow across the upper bounding surface, is given in Sec. II. Numerical results for the relaxation regimes caused by the vertical temperature gradient, describing orientational relaxation of the director, velocity, and temperature, are given in Sec. III. Conclusions are summarized in Sec. IV.

II. FORMULATION OF THE BALANCE OF THE MOMENTUM AND TORQUE EQUATIONS AND CONDUCTIVITY EQUATION FOR NEMATIC FLUIDS

To fix ideas and notation, we shall be considering a HOLC film delimited by two horizontal and two lateral surfaces at mutual distance d on scale on the order of micrometers, with the heat flow q

$$\lambda_{\perp}\left(\frac{\partial T(t,x,z)}{\partial z}\right)_{z=d}=q, \tag{1}$$

across the upper restricted boundary, whereas on the rest boundaries the temperature is kept constant,

$$T_{0\le x\le d,z=0}=T_{x=0,0<z<d}=T_{x=d,0<z<d}=T_{\mathrm{lw}}. \tag{2}$$

Here $\lambda_{\perp}$ is the heat conductivity coefficient perpendicular to the director $\hat{\mathbf{n}}=(n_x,0,n_z)=\sin\theta\hat{\mathbf{i}}+\cos\theta\hat{\mathbf{k}}$, where $\theta\equiv\theta(t,x,z)$ denotes the polar angle, i.e., the angle between

*Author to whom correspondence should be addressed; avz02@yahoo.com; www.ipme.ru

†avak@microm.ipme.ru; www.ipme.ru

the direction of the director $\hat{\mathbf{n}}(t,\mathbf{r})$ and the normal $\hat{\mathbf{k}}$ to the boundary surfaces, and T_{lw} is the temperature on the lower and two lateral solid surfaces. The coordinate system defined by our task assumed that the director $\hat{\mathbf{n}}$ is in the XZ plane, where $\hat{\mathbf{i}}$ is the unit vector directed parallel to the restricted surfaces, which coincides with the planar director orientation on the upper restricted surface ($\hat{\mathbf{i}} \| \hat{\mathbf{n}}_{z=d}$), and $\hat{\mathbf{j}}=\hat{\mathbf{k}}\times\hat{\mathbf{i}}$. Therefore, the hybrid aligned nematic state contains a gradient of $\nabla\theta$ from homeotropic orientation at the lower surface to planar orientation at the upper and lateral surfaces, i.e.,

$$\theta_{0<x<d,z=0} = \theta_{x=0,0\le z<d} = \theta_{x=d,0\le z<d} = 0,$$

$$\theta_{0\le x\le d,z=d} = \frac{\pi}{2}. \tag{3}$$

Taking into account that the size of the LC film $d \sim 1-5$ μm, one can assume that the mass density ρ_m =const across the HOLC cell, and one deals with an incompressible fluid. Incompressibility condition $\nabla\cdot\mathbf{v}=0$ assumes that

$$u_{,x} + w_{,z} = 0, \tag{4}$$

where $u \equiv v_x(t,x,z)$ and $w \equiv v_z(t,x,z)$ are the components of the vector $\mathbf{v}$, and $u_{,x}=\frac{\partial u}{\partial x}$.

The dimensionless hydrodynamic equations describing the reorientation of the LC phase in 2D case, when there exists a heat flow across the upper restricted surface, whereas the temperature on the rest surfaces is kept constant, can be derived from the dimensionless torque balance equation $\mathbf{T}_{\mathrm{el}}+\mathbf{T}_{\mathrm{vis}}+\mathbf{T}_{\mathrm{tm}}=0$, where $\mathbf{T}_{\mathrm{el}}=\mathcal{B}_{\mathrm{el}}\hat{\mathbf{j}}$ is the elastic [2], $\mathbf{T}_{\mathrm{vis}}=\mathcal{B}_{\mathrm{vis}}\hat{\mathbf{j}}$ is the viscous [3,6–8], and $\mathbf{T}_{\mathrm{tm}}=\delta_1\mathcal{B}_{\mathrm{tm}}\hat{\mathbf{j}}$ is the thermomechanical [3,5–8] dimensionless torques, respectively (for details, see the Appendix), the dimensionless Navier-Stokes equation for the velocity field $\mathbf{v}=u\hat{\mathbf{i}}+w\hat{\mathbf{k}}$ [13],

$$\delta_2\frac{du}{d\tau} = \sigma_{xx,x} + \sigma_{zx,z},$$

$$\delta_2\frac{dw}{d\tau} = \sigma_{zz,z} + \sigma_{xz,x}, \tag{5}$$

where $\frac{du}{d\tau}$ is the material derivative of the velocity component u, $\sigma_{ij}=P\delta_{ij}+\sigma_{ij}^{\mathrm{el}}+\sigma_{ij}^{\mathrm{vis}}+\sigma_{ij}^{\mathrm{tm}}(i,j=x,z)$ is the stress tensor (ST) of the LC system, P is the hydrostatic pressure in the HOLC cell, and $\sigma_{ij}^{\mathrm{el}}$, $\sigma_{ij}^{\mathrm{vis}}$, and $\sigma_{ij}^{\mathrm{tm}}$ are the dimensionless ST components corresponding to the elastic, viscous, and thermomechanical forces (see the Appendix), respectively. The dimensionless equation for the heat conduction, due to the growth of the temperature difference $\Delta\chi=\chi_2-\chi_1$ on the LC cell boundaries, excited both by the velocity field and the heat flow, takes the form (for details, see also the Appendix) [11]

$$\delta_3\frac{d\chi}{d\tau} = \mathcal{D}_1\chi_{,xx} + \mathcal{D}_2\chi_{,zz} + 2\mathcal{D}_3\chi_{,xz} + \mathcal{D}_{1,x}\chi_{,x} + \mathcal{D}_{2,z}\chi_{,z} - \mathcal{D}_{3,x}\chi_{,z} - \mathcal{D}_{3,z}\chi_{,x}, \tag{6}$$

where $\mathcal{D}_1=\lambda n_x^2+n_z^2$, $\mathcal{D}_2=\lambda n_z^2+n_x^2$, and $\mathcal{D}_3=(\lambda-1)n_xn_z$, are the functions of the polar angle θ, $\lambda=\lambda_{\|}/\lambda_{\perp}$ is the dimensionless parameter, and $\lambda_{\|}$ is the heat conductivity coefficient parallel to the director. Here $\chi\equiv\chi(\tau,x,z)=T(\tau,x,z)/T_{\mathrm{NI}}$ is the dimensionless temperature, T_{NI} is the nematic-isotropic transition temperature, $[\chi_2,\chi_1]$ is the temperature interval across the LC sample and belongs to the nematic stability range, $\chi_{,x}=\frac{\partial\chi}{\partial x}$, $\chi_{,xx}=\frac{\partial^2\chi}{\partial x^2}$, $\delta_1=\xi\frac{T_{\mathrm{NI}}}{K_1}$, $\delta_2=\frac{\rho_m K_1}{\gamma_1^2}$, and $\delta_3=\frac{\rho_m C_p K_1}{\gamma_1\lambda_{\perp}}$ are three parameters of the system, K_1 and K_3 are the splay and bend elastic constants of the LC phase, $\xi\sim 10^{-12}$ J/mK is the thermomechanical constant [2,3,7], γ_1 and γ_2 are the rotational viscosity coefficients, and C_p is the heat capacity; whereas $\tau=(\frac{K_1}{\gamma_1 d^2})t$ is the dimensionless time, $\bar{z}=\frac{z}{d}$ is the dimensionless distance away from the lower solid surface, and $\bar{x}=\frac{x}{d}$ is the dimensionless space variable corresponding to x axis. Notice that a single-constant approximation for the thermomechanical coupling tensor has been proposed [3], as well as the overbars in the space variables x and z have been eliminated. In the following, we are focused primarily on the heat conduction regime in the HOLC cell, which assume that across the upper surface the heat flow is restricted [Eq. (1)], whereas on the rest surfaces the temperature is kept constant [Eq. (2)]. Physically, this means that across the LC sample, a temperature gradient ∇T may be built up, directed from the cooler to the warmer surfaces, under the action of the hydrodynamic flow, and excited by the heat flow q across to the upper boundary.

To be able to observe the formation of the temperature difference $\Delta\chi$ across the LC sample, under the action of the heat flow q, when the heating occurs during some times τ_{in}, we consider the dimensionless analog of the torque balance equation (for details, see the Appendix),

$$\begin{aligned} n_x\frac{dn_z}{d\tau} - n_z\frac{dn_x}{d\tau} + \frac{1}{2}(w_{,x}-u_{,z}) + n_xn_z(w_{,z}-u_{,x})\gamma \\ + (n_x^2-n_z^2)(u_{,z}+w_{,x})\gamma + n_z\mathcal{M}_{0,x} - n_x\mathcal{M}_{0,z} \\ + \frac{K_3}{K_1}(n_zh_{,z}-n_xh_{,x}) + \delta_1\chi_{,x}\left[-\frac{1}{2}n_z\mathcal{M}_0 - n_zM_{xx}\right. \\ \left. + n_x^2(n_xM_{zz}-M_{xx}n_z+2n_xM_{xz})\right] + \delta_1\chi_{,z}\left[\frac{1}{2}n_x\mathcal{M}_0\right. \\ \left. + n_xM_{zz} + n_z^2(n_xM_{zz}-M_{xx}n_x-2n_zM_{xz})\right] = 0, \end{aligned} \tag{7}$$

where $\gamma=\gamma_2/\gamma_1$, $\mathcal{M}_0=\nabla\cdot\hat{\mathbf{n}}$ is the scalar invariant of the tensor $\mathbf{M}=\frac{1}{2}[\nabla\hat{\mathbf{n}}+(\nabla\hat{\mathbf{n}})^{\mathrm{T}}]$, and $\mathcal{M}_{0,i}=\frac{\partial\mathcal{M}_0}{\partial x_i}(i=x,z)$. Here $(\nabla\hat{\mathbf{n}})^{\mathrm{T}}$ is the transposition of $\nabla\hat{\mathbf{n}}$.

Now, the reorientation of the director in the LC film confined between two horizontal and two vertical solid surfaces, when the relaxation regime is governed by the viscous, elastic, and thermomechanical forces, and with accounting for the flow, can be obtained by solving the system of the nonlinear partial differential Eqs. (5)–(7) with the appropriate dimensionless boundary conditions for the polar angle

$$\theta_{0<x<1,z=0} = \theta_{x=0,0\le z<1} = \theta_{x=1,0\le z<1} = 0,$$

$$\theta_{0\le x\le 1,z=1} = \frac{\pi}{2}, \tag{8}$$

velocity

$$u_{0<x<1,z=0} = u_{x=0,0\le z<1} = u_{x=d,0\le z<1} = u_{0\le x\le 1,z=1} = 0,$$

$$w_{0<x<1,z=0} = w_{x=0,0\le z<1} = w_{x=d,0\le z<1} = w_{0\le x\le 1,z=1} = 0, \tag{9}$$

and temperature

$$\chi_{0\le x\le 1,z=0} = \chi_{x=0,0<z<1} = \chi_{x=1,0<z<1} = \chi_{\mathrm{lw}},$$

$$\left(\frac{\partial \chi(\tau,x,z)}{\partial z}\right)_{0\le x\le 1,z=1} = \bar{Q}. \tag{10}$$

Here $\chi_{\mathrm{lw}}=\frac{T_{\mathrm{lw}}}{T_{\mathrm{NI}}}$, and $\bar{Q}=-\frac{qd}{T_{\mathrm{NI}}\lambda_{\perp}}$ is the dimensionless heat flow across the upper restricted surface. Recently, laser-induced heating was used to inject energy $\bar{Q}$ across the bounding surface at the microscopic scale [14]. In that case, the LC sample was heated by a laser beam focused, for instance, on the upper bounding surface $(z=1, x=x_0)$, with intensity $\mathcal{I}(x)=\frac{2P_0}{\pi\omega_0^2}\exp(-\frac{2(x-x_0)^2}{\omega_0^2})$, where P_0 is the laser power, and ω_0 is the Gaussian spot size. Taking into account that the total absorbed laser power is $P_{\mathrm{in}}=\alpha\mathcal{I}(x)$, the heat flow across the upper restricted surface can be written as

$$\bar{Q} = Q\exp\left(-\frac{2(x-x_0)^2}{\bar{\omega}_0^2}\right)\mathcal{H}[\tau_{\mathrm{in}}-\tau], \tag{11}$$

where α is the absorption coefficient, $\bar{\omega}_0=\frac{\omega_0}{d}$, $Q=-\frac{2\alpha P_0 d}{\pi\omega_0^2\lambda_{\perp}T_{\mathrm{NI}}}$ is the dimensionless heat flow's coefficient, $\mathcal{H}[\tau_{\mathrm{in}}-\tau]$ is the Heaviside step function, and τ_{in} is the duration of the energy injection into the LC sample.

On the other hand, when the director $\hat{\mathbf{n}}$ is strongly homeotropically anchored to the lower and two lateral surfaces, and homogeneously to the upper restricted surfaces the polar angle has to satisfy the boundary conditions (8) and its initial orientation is chosen equal to $\theta(\tau=0,x,z)=\theta_{\mathrm{elast}}(x,z)$, where $\theta_{\mathrm{elast}}(x,z)$ is obtained from Eq. (7), with $u_{,x}=u_{,z}=w_{,x}=w_{,z}=\chi_{,x}=\chi_{,z}=0$, and the boundary and initial conditions in the form of Eqs. (8), and $\theta(\tau=0,x,z)=\frac{\pi}{2}z$, for $0\le z<1$, and $\theta(\tau=0,x,0)=0$, for $\forall x$, respectively, and then, under the action of the viscous, elastic, and thermomechanical forces, allowed to relax to its equilibrium value $\theta_{\mathrm{eq}}(x,z)$.

For the case of 4−cyano−4′−pentylbiphenyl(5CB), at temperature corresponding to nematic phase, the set of parameters involved in Eqs. (5)–(7) are $\delta_1\sim 24$, $\delta_2\sim 2\times 10^{-6}$, and $\delta_3\sim 6\times 10^{-4}$ (for details, see Refs. [5,8]). Using the fact that δ_2 and δ_3 are $\ll 1$, the Navier-Stokes [Eqs. (5)] and the heat conduction [Eq. (6)] equations can be considerably simplified. Thus, the whole left-hand side of Eqs. (5) and (6) can be neglected and these equations take the form

$$\sigma_{xx,x} + \sigma_{zx,z} = 0,$$

$$\sigma_{zz,z} + \sigma_{xz,x} = 0, \tag{12}$$

and

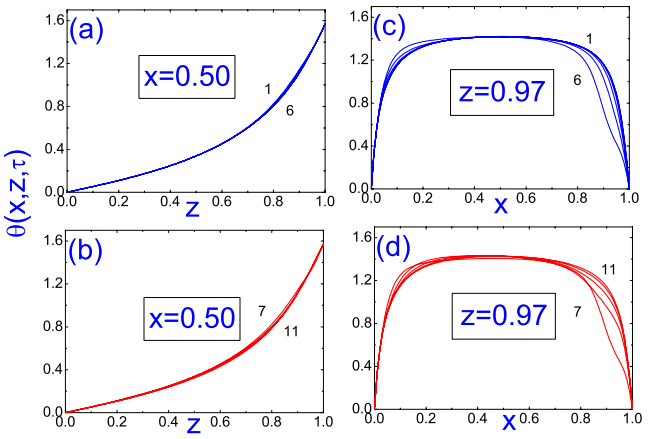

FIG. 1. (Color online) (a) Plot of relaxation of the polar angle $\theta(\tau,x=0.5,z)$ (in rad) to its equilibrium distribution $\theta_{\mathrm{eq}}(x=0.5,z)$ in the middle part of the HOLC cell, under the influence of the dimensionless heat flow $Q=0.44(\sim 3.7\times 10^{-3}$ mW/μm$^2)$, caused by the laser beam, at different times $\tau_1=0.000\,42$ [curve(1)], …, $\tau_6=0.0134$ [curve(6)], respectively. (b) The same as in (a), but the sequence of times is $\tau_7=0.014$ [curve(7)], …, $\tau_{11}=\tau_{\mathrm{R}}=0.22$ [curve(11)], respectively. (c) and (d) Plot of relaxation of the polar angle $\theta(\tau,x,z=0.97)$ to its equilibrium distribution $\theta_{\mathrm{eq}}(x,z=0.97)$ along the width of the HOLC $(0\le x\le 1)$ in the vicinity of the upper warmer restricted surface $(z=0.97)$, at different times $\tau_1=0.000\,42$ [curve(1)], …, $\tau_{11}=\tau_{\mathrm{R}}=0.22$ [curve(11)], respectively.

$$\mathcal{D}_1\chi_{,xx} + \mathcal{D}_2\chi_{,zz} + 2\mathcal{D}_3\chi_{,xz} + \mathcal{D}_{1,x}\chi_{,x} + \mathcal{D}_{2,z}\chi_{,z} - \mathcal{D}_{3,x}\chi_{,z} - \mathcal{D}_{3,z}\chi_{,x} = 0, \tag{13}$$

where $\mathcal{D}_{1,x}=2(\lambda n_x n_{x,x}+n_z n_{z,x})$, $\mathcal{D}_{2,z}=2(\lambda n_z n_{z,z}+n_x n_{x,z})$, and $\mathcal{D}_{3,z}=(\lambda-1)[n_z n_{x,x}+n_x n_{z,x}]$ are the functions of the polar angle θ.

III. ORIENTATIONAL RELAXATION OF THE DIRECTOR, VELOCITY, AND TEMPERATURE FIELDS IN THE HOLC CELL

The relaxation of the director $\hat{\mathbf{n}}$ to its equilibrium orientation $\hat{\mathbf{n}}_{\mathrm{eq}}$, which is described by the polar angle $\theta(\tau,x,z)$ changing from the initial condition $\theta(\tau=0,x,z)=\theta_{\mathrm{elast}}(x,z)$ to $\theta_{\mathrm{eq}}(x,z)$ [see Figs. 1(a)–1(d)], both velocities $u(\tau,x,z)=v_x(\tau,x,z)$ [see Figs. 2(a)–2(d)] and $w(\tau,x,z)=v_z(\tau,x,z)$ [see Figs. 3(a)–3(d)] and temperature $\chi(\tau,x,z)$ [see Figs. 4(a)–4(d)], under the action of the temperature gradient ∇T, caused by the heat flow across the upper restricted surface, whereas on the rest bounding surfaces the temperature is kept constant, can be obtained by solving the system of the nonlinear partial differential Eqs. (7), (12), and (13), together with the boundary conditions (8)–(10), by means of the numerical relaxation method [15]. For that aim, the system of Eqs. (12) and (13) should be rewritten in the form

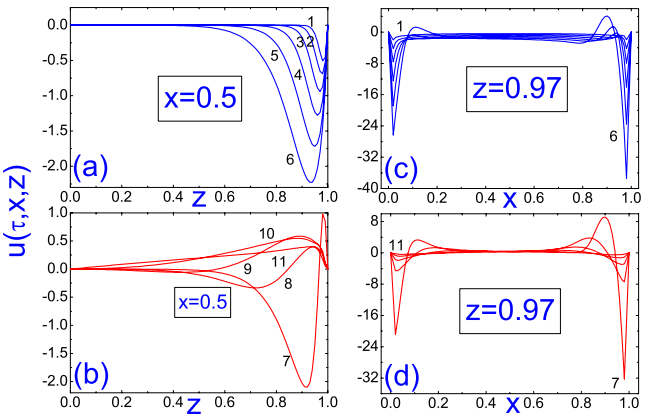

FIG. 2. (Color online) (a)–(d) Plot of relaxation of the velocity $u(\tau,x,z)$ to its equilibrium distribution $u_{eq}(x,z)$ across the HOLC. The sequence of times is the same as in Figs. 1(a)–1(d).

$$\frac{\partial u}{\partial \tau} = \mathcal{B}_{11}u_{,xx} + \mathcal{B}_{12}u_{,zz} + \mathcal{B}_{13}u_{,xz} + \mathcal{B}_{14}w_{,xx} + \mathcal{B}_{15}w_{,x} + \mathcal{B}_{16}(u_{,z} + w_{,x}) + \gamma\left(n_x\frac{dn_x}{d\tau}\right)_{,x} + \frac{\gamma-1}{2}\left(n_z\frac{dn_x}{d\tau}\right)_{,z} + \frac{\gamma+1}{2}\left(n_x\frac{dn_z}{d\tau}\right)_{,z} + \delta_1\mathcal{F}_1(\chi),$$

$$\frac{\partial w}{\partial \tau} = \mathcal{B}_{21}w_{,xx} + \mathcal{B}_{22}w_{,zz} + \mathcal{B}_{23}w_{,xz} + \mathcal{B}_{24}u_{,zz} - \mathcal{B}_{25}w_{,z} + \mathcal{B}_{26}(u_{,z} + w_{,x}) + \gamma\left(n_z\frac{dn_z}{d\tau}\right)_{,z} + \frac{\gamma-1}{2}\left(n_x\frac{dn_z}{d\tau}\right)_{,x} + \frac{\gamma+1}{2}\left(n_z\frac{dn_x}{d\tau}\right)_{,x} + \delta_1\mathcal{F}_2(\chi), \tag{14}$$

$$\frac{\partial \chi}{\partial \tau} = \mathcal{D}_1\chi_{,xx} + \mathcal{D}_2\chi_{,zz} + 2\mathcal{D}_3\chi_{,xz} + \mathcal{D}_{1,x}\chi_{,x} + \mathcal{D}_{2,z}\chi_{,z} - \mathcal{D}_{3,x}\chi_{,z} - \mathcal{D}_{3,z}\chi_{,x}, \tag{15}$$

where the coefficients $\mathcal{B}_{ij}(i=1,2;j=1,\ldots,6)$ are the hydrodynamic functions, whereas the coefficients $\mathcal{F}_i(i=1,2)$ are the thermomechanical functions and are collected in the Appendix. In the calculations, the relaxation criterion $\epsilon=|[\theta_{(m+1)}(\tau,x,z)-\theta_{(m)}(\tau,x,z)]/\theta_{(m)}(\tau,x,z)|$ was chosen equal to be 10^{-4}, and the numerical procedure was then carried out until a prescribed accuracy was achieved. Here m is the iteration number and τ_R is the relaxation time of the system.

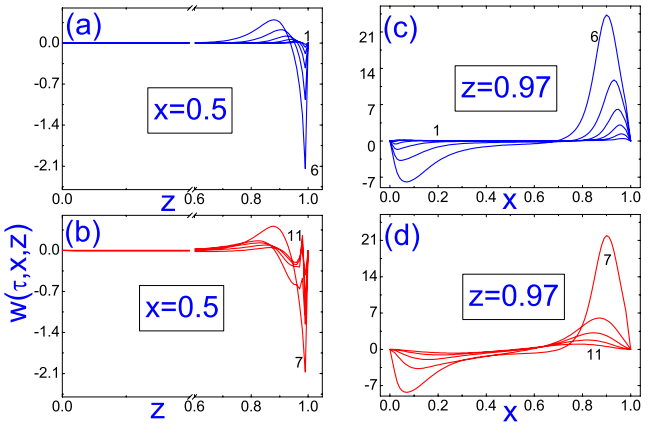

FIG. 3. (Color online) (a)–(d) Plot of relaxation of the velocity $w(\tau,x,z)$ to its equilibrium distribution $w_{eq}(x,z)$ across the HOLC. The sequence of times is the same as in Figs. 1(a)–1(d).

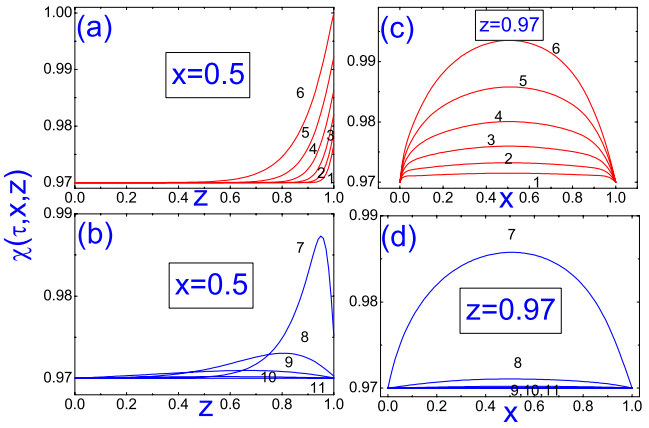

FIG. 4. (Color online) (a)–(d) Plot of relaxation of the temperature $\chi(\tau,x,z)$ to its equilibrium distribution $\chi_{eq}(x,z)$ across the HOLC. The sequence of times is the same as in Figs. 1(a)–1(d).

A. Slow heating regime

The relaxation process of the polar angle $\theta(\tau,x,z)$ in the middle part of the dimensionless HOLC cell $(x=0.5)$ [see Figs. 1(a) and 1(b)] to its equilibrium distribution $\theta_{eq}(x=0.5,z)$, under the influence of the dimensionless heat flow $Q=0.44(\sim 3.7\times 10^{-3}\ \mathrm{mW}/\mu\mathrm{m}^2)$, caused by the laser beam focused on the upper bounding surface, at different times $\tau_1=0.000\,42(\sim 54\ \mu\mathrm{s})$ [curve(1)], …, $\tau_{11}=\tau_R=0.22(\sim 30\ \mathrm{ms})$ [curve(11)], is shown in Figs. 1(a) and 1(b), respectively. Here we use times $\tau_k=2^{k-1}\tau_1$, for $k=1,\ldots,6$, whose values increase from curve 1 to curve 6, and $\tau_1=0.000\,42$, and $\tau_k=2^{k-7}\tau_7$, for $k=7,\ldots,11$, whose values increase from curve 7 to curve 11, and $\tau_7=0.014$, respectively, τ_R denotes the relaxation time of the system, and $\tau_{in}\sim\tau_6\sim 0.0134(\sim 1.9\ \mathrm{ms})$ is the duration of the energy injection into the HOLC cell across the upper restricted surface by the infrared laser with the power $P_0=14.3$ mW. The relaxation of the polar angle is characterized by the monotonic increase θ from $\theta(x=0.5,z=0)=0$, on the lower cooler restricted surface, to $\theta(x=0.5,z=1)=\frac{\pi}{2}$, on the upper warmer restricted surface, respectively. The relaxation of the polar angle $\theta(\tau,x,z=0.97)$ to its equilibrium distribution $\theta_{eq}(x,z=0.97)$ along the width of the HOLC $(0\le x\le 1)$ in the vicinity of the upper warmer restricted surface $(z=0.97)$, at different times $\tau_1=0.000\,42(\sim 54\ \mu\mathrm{s})$ [curve(1)], …, $\tau_{11}=\tau_R=0.22(\sim 30\ \mathrm{ms})$ [curve(11)], is shown in Figs. 1(c) and 1(d), respectively. The relaxation process is characterized by the nonsymmetric profile of $\theta(\tau,x,z=0.97)$ with respect to the middle part $(x=0.5)$ of the HOLC cell, which caused by the nonsymmetric effect both the velocity fields $u(\tau,x,z)$

[see Figs. 2(c) and 2(d)] and $w(\tau,x,z)$ [see Figs. 3(c) and 3(d)], respectively.

The maximum of the absolute magnitudes of both dimensional velocities $v_x(\tau,x,z)=(\frac{\gamma_1 d}{K_1})u(\tau,x,z)$ and $v_z(\tau,x,z)=(\frac{\gamma_1 d}{K_1})w(\tau,x,z)$ in the HOLC cell, at the initial stage of the relaxation process are equal to 1.2 mm/s and 0.88 mm/s, for the horizontal and vertical components [see Figs. 3(c) and 4(c)], at $\Delta\chi_{max}=0.03(\sim 9.3$ K), respectively. The relaxation process of the temperature field $\chi(\tau,x,z)$ in the middle part of the dimensionless HOLC cell ($x=0.5$) to its equilibrium distribution $\chi_{eq}(x=0.5,z)$, under the influence of the dimensionless heat flow $Q=0.44(\sim 3.7\times 10^{-3}$ mW/μm^2), caused by the laser beam, at different times $\tau_1=0.000\,42$ [curve(1)], …, $\tau_{11}=\tau_R=0.22$ [curve(11)], is shown in Figs. 4(a) and 4(b), respectively.

The evolution of the dimensionless temperature field $\chi(\tau,x=0.5,z)$ is characterized by the temperature growth on the upper restricted surface ($z=1$), from $\chi_{z=1}=0.97(\sim 298$ K) to $\chi_{z=1}=1.0(\sim 307.3$ K), during the first part of the relaxation process [curves from (1) to (6)] [see Fig. 4(a)], with the following temperature decreasing, from $\chi_{z=1}=1.0(\sim 307.3$ K) to $\chi_{z=1}=0.97(\sim 298$ K), after switching off the laser power [see Fig. 4(b)]. Here the value of $\tau_{in}=\tau_6\sim 0.0134(\sim 1.9$ ms). The second part of the relaxation process of $\chi(\tau,x=0.5,z)$ ($\tau\geq\tau_6$) is characterized by much faster cooling down of the upper restricted surface than the rest bulk of the LC sample [see Fig. 4(b)]. The relaxation of the temperature field $\chi(\tau,x,z=0.97)$ to its equilibrium distribution $\chi_{eq}(x,z=0.97)$ along the width of the HOLC ($0\leq x\leq 1$) in the vicinity of the upper warmer restricted surface ($z=0.97$), at different times $\tau_1=0.000\,42$ [curve(1)], …, $\tau_{11}=\tau_R=0.22$ [curve(11)], is shown in Figs. 4(c) and 4(d), respectively. That relaxation process is characterized by symmetric growth of the profile $\chi(\tau,x,z=0.97)$ with respect to the middle part ($x=0.5$) of the HOLC cell. Such symmetric evolution of the temperature field can be explained by much faster relaxation of $\chi(\tau,x,z)$ to $\chi_{eq}(x,z)$, then relaxation both of the director and velocity fields to their equilibrium distributions across the HOLC cell, and—as results—the weak effect of these fields on χ.

B. Fast heating regime

The equilibrium distribution $\theta_{eq}(x=0.5,z)$ both across the middle part and in the vicinity of the upper restricted surfaces, under the influence of the dimensionless heat flow $Q=3.54(\sim 2.95\times 10^{-2}$ mW/μm^2) [which is in eight times greater than Q in the first case (a)], caused by the laser beam focused on the upper bounding surface, is shown in Figs. 5(a) and 5(b), respectively.

Here the duration τ_{in} of the energy injection into the HOLC cell across the upper restricted surface is equal to 0.000 08(~ 11 μs) and during that time the temperature on the upper restricted surface growth from $\chi_{z=1}(\tau=0)=0.97(298$ K) to $\chi_{z=1}(\tau=\tau_2=\tau_{in}\sim 0.000\,08)=1.0(307.3$ K) [see Fig. 6(a)], with the following cooling down to $\chi_{z=1}(\tau=\tau_R=0.064)=0.97(298$ K). Note that the duration of the laser pulse, at fixed power $P_0=115$ mW, is limited by the condition that the higher temperature on the upper

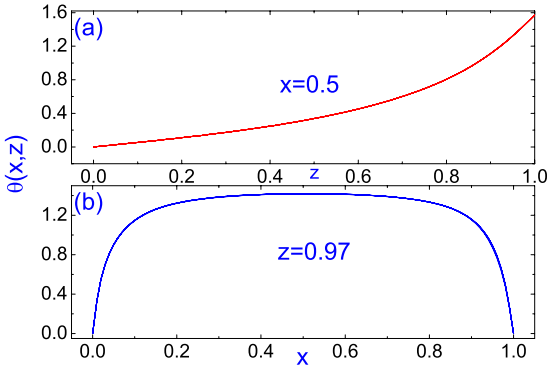

FIG. 5. (Color online) (a) The equilibrium distribution of the angle $\theta_{eq}(x=0.5,z)$ in the middle part of the HOLC cell, under influence of the dimensionless heat flow $Q=3.54(\sim 2.95\times 10^{-2}$ mW/μm^2), caused by the laser beam. (b) The equilibrium distribution $\theta_{eq}(x,z=0.97)$ along the width of the HOLC ($0\leq x\leq 1$) in the vicinity of the upper warmer restricted surface ($z=0.97$), under the same as in (a) conditions.

bounding surface $\chi_{z=1}$ must fall within the nematic stability range. The relaxation process of the temperature field $\chi(\tau,x=0.5,z)$ in the middle part of the dimensionless HOLC cell ($x=0.5$) [see Figs. 6(a) and 6(b)] to its equilibrium distribution $\chi_{eq}(x=0.5,z)$, under the influence of the dimensionless heat flow $Q=3.54(\sim 2.95\times 10^{-2}$ mW/μm^2), caused by the laser beam, at different times $\tau_1=0.000\,04(\sim 6$ μs) [curve(1)], …, $\tau_{12}=\tau_R=0.064(\sim 8.7$ ms) [curve(12)], is shown in Figs. 6(a) and 6(b), respectively. Here $\tau_{in}=\tau_2\sim 0.000\,08(\sim 11$ μs) is the duration of the energy injection into the HOLC cell across

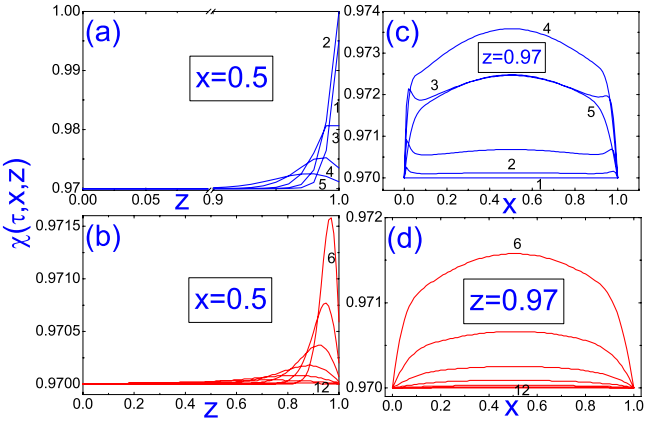

FIG. 6. (Color online) (a) Plot of relaxation of the temperature field $\chi(\tau,x=0.5,z)$ to its equilibrium distribution $\chi_{eq}(x=0.5,z)$ in the middle part of the HOLC cell, under the influence of the dimensionless heat flow $Q=3.54(\sim 2.95\times 10^{-2}$ mW/μm^2), caused by the laser beam, at different times $\tau_1=0.000\,04$ [curve(1)], …, $\tau_5=0.0006$ [curve(5)], respectively. (b) The same as in (a), but the sequence of times is $\tau_6=0.001$ [curve(6)], …, $\tau_{12}=\tau_R=0.064$ [curve(12)], respectively. (c) and (d) Plot of relaxation of the temperature field $\chi(\tau,x,z=0.97)$ to its equilibrium distribution $\chi_{eq}(x,z=0.97)$ along the width of the HOLC ($0\leq x\leq 1$) in the vicinity of the upper warmer restricted surface ($z=0.97$), at different times $\tau_1=0.000\,04$ [curve(1)], …, $\tau_{12}=\tau_R=0.064$ [curve(12)], respectively.

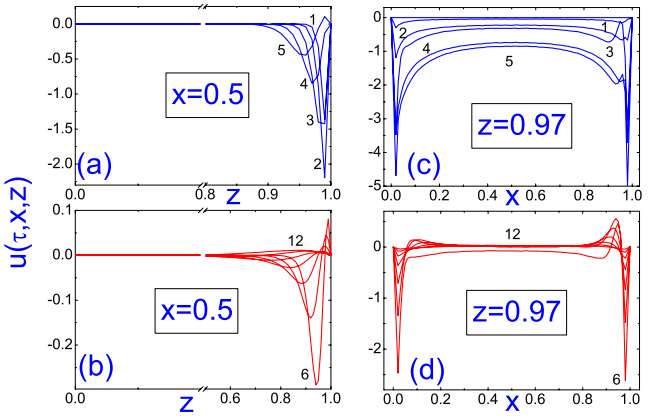

FIG. 7. (Color online) (a)–(d) Plot of relaxation of the velocity $u(\tau,x,z)$ to its equilibrium distribution $u_{eq}(x,z)$ across the HOLC. The sequence of times is the same as in Figs. 6(a)–6(d).

the upper restricted surface by the infrared laser with the power $P_0=115$ mW. The relaxation of the temperature field $\chi(\tau,x,z=0.97)$ to its equilibrium distribution $\chi_{eq}(x,z=0.97)$ along the width of the HOLC $(0\leq x\leq 1)$ in the vicinity of the upper warmer restricted surface $(z=0.97)$, at different times $\tau_1=0.000\,04(\sim 6\ \mu s)$ [curve(1)], …, $\tau_{12}=\tau_R=0.064(\sim 8.7$ ms) [curve(12)], is shown in Figs. 6(c) and 6(d), respectively. Here we use times $\tau_k=2^{k-1}\tau_1$, for $k=1,\ldots,5$, whose values increase from curve 1 to curve 5, and $\tau_1=4\times 10^{-5}$, and $\tau_k=2^{k-6}\tau_6$, for $k=6,\ldots,12$, whose values increase from curve 6 to curve 12, and $\tau_6=0.001$, respectively. That relaxation process is characterized by symmetric growth of the profile $\chi(\tau,x,z=0.97)$ with respect to the middle part $(x=0.5)$ of the HOLC cell. Such symmetric evolution of the temperature field can be explained by much faster relaxation of $\chi(\tau,x,z)$ to $\chi_{eq}(x,z)$, then both $\theta(\tau,x,z)$, and $v(\tau,x,z)$ to their equilibrium values. The evolution of the velocity field $\mathbf{v}=u\hat{\mathbf{i}}+w\hat{\mathbf{k}}$ to its equilibrium distribution in the HOLC cell is shown in Figs. 7(c), 7(d), 8(c), and 8(d), respectively. The relaxation of $u(\tau,x,z)$ in the middle part of the dimensionless HOLC cell $(x=0.5)$ [see Fig. 7(a)] to its equilibrium distribution $u_{eq}(x=0.5,z)$, under the influence of the dimensionless heat flow $Q=3.54(\sim 2.95\times 10^{-2}$ mW/μm$^2)$, caused by the laser beam, at different times $\tau_1=0.000\,04(\sim 6\ \mu s)$ [curve(1)], …, $\tau_{12}=\tau_R=0.064(\sim 8.7$ ms) [curve(12)], is shown in Figs. 7(a) and 7(b), respectively. Here $\tau_{in}\sim 0.000\,08(\sim 11\ \mu s)$ is the duration of the energy injection into the HOLC cell across the upper restricted surface by the infrared laser with the power $P_0=115$ mW. The relaxation of $u(\tau,x=0.5,z)$ [see Fig. 7(a)] is characterized by the strong increase of $|u(\tau,x=0.5,z)|$, from $|u(\tau=0)|=0$ to $|u(\tau=\tau_2=\tau_{in})|\sim 2.5$, within the first part of the relaxation process $(\sim 11\ \mu s)$, in the vicinity of the upper warmer restricted surface, with following decrease up to ~ 0, during the rest time term $\tau_R-\tau_2\sim 0.064(\sim 8.7\ \mu s)$, respectively. The relaxation of $w(\tau,x=0.5,z)$ to its equilibrium distribution across the HOLC is characterized by oscillating behavior of $w(\tau,x=0.5,z)$ in the vicinity of the upper warmer restricted surface [see Figs. 8(a) and 8(b)]. Note that the x asymmetry during the relaxation of the director field described by the polar angle $\theta(\tau,x,z)$ (see Figs. 1(c) and 1(d)] is caused by the asymmetric acting of the velocity field. Note also that under the influence of the heat flow across the upper restricted surface, only approximately 40% of the LC sample close to the upper warmer restricted surface is involved in the moving process, whereas the rest amount of the LC sample is kept unmoved during the full relaxation term $\tau_R\sim 0.64$. The maximum of both the absolute magnitudes of the dimension velocities $v_x(\tau,x,z)=(\frac{\gamma_1 d}{K_1})u(\tau,x,z)$ and $v_z(\tau,x,z)=(\frac{\gamma_1 d}{K_1})w(\tau,x,z)$ in the HOLC cell, at the initial stage of the relaxation process are equals to 0.2 mm/s and 0.05 mm/s, for horizontal and vertical components [see Figs. 7(c) and 8(c)], at $\Delta\chi_{max}=0.03(\sim 9.3$ K), respectively.

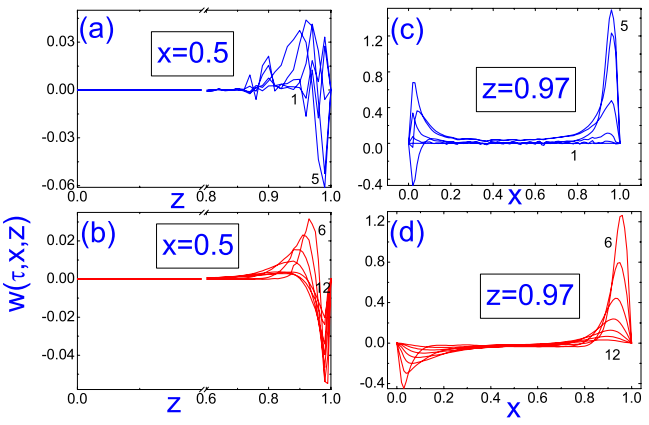

FIG. 8. (Color online) (a)–(d) Plot of relaxation of the velocity $w(\tau,x,z)$ to its equilibrium distribution $w_{eq}(x,z)$ across the HOLC. The sequence of times is the same as in Figs. 6(a)–6(d).

IV. CONCLUSION

In summary, we have investigated the relaxation of director $\hat{\mathbf{n}}(t,x,z)$, velocity $\mathbf{v}(t,x,z)$, and temperature $\chi(t,x,z)$ in the 2D HOLC cell to their equilibrium values, under the influence of the heat flow directed normal to the upper bounding surfaces, when the rest bounding surfaces of the LC cell are kept at constant temperature. In our case, the upper LC layer is heated by an infrared laser beam, and the dynamics of heating occurs with two distinct time scales: (i) a fast time, with the duration of the laser pulse in $\tau_{in}\sim 11\ \mu s$, and the laser power in $P_0=115$ mW, and (ii) a slow time scale, with the duration of the laser pulse in $\tau_{in}\sim 1.9$ ms, and the laser power in $P_0=14.3$ mW, respectively. In both these cases, the duration of the laser pulse, at fixed power in $P_0=14.3$ mW and $P_0=115$ mW, is limited by the condition that the higher temperature on the upper bounding surface must fall within the nematic stability range. Our calculations based upon the nonlinear extension of the classical Ericksen-Leslie theory shows that the HOLC material under the influence of the heat flow, after some time, more than the time of relaxation, for instance, of the director field in the HOLC cell, settles down to the rest state regime, where the horizontal u and vertical w components of velocity vector are equal to zero, and the temperature field across the LC cell finally reaches the value of temperature on the lower and both lateral bounding surfaces. Note that in the case of

the fast heating regime (i), one deals with the heating which is characterized by "shallow" heating of the LC layers in the vicinity of the upper bounding surface up to 40% of the full LC sample, whereas in the case of the slow heating regime (ii), one deals with the "deeper" heating of the LC layers up to 60% of the LC sample far from the upper warmer restricted surface, respectively. Our calculations shows that the 2D HOLC material under the influence of the heat flow directed normal to the upper restricted surface, after some time, more than the relaxation time, for instance, of the director field in the HOLC cell, settles down to the rest state regime, where the horizontal and vertical components of the velocity vector are equals to zero, and the temperature field across the LC cell finally reaches the value of temperature on the lower and two lateral bounding surfaces.

We believe that the present investigation can shed some light on the problem of the reorientation process in the HOLC cell under the influence of the heat flow. We also believe that the paper shows not only some useful routes for estimating the relaxation times but also analyzing the remaining problems associated with LC's device stability, efficiency, and lifetime.

ACKNOWLEDGMENT

We acknowledge the financial support of the Russian Funds for Fundamental Research (Grant No. 09-02-00010-a).

APPENDIX: TORQUES AND STRESS TENSOR COMPONENTS

The torque balance equation can be derived from the dimensionless balance of elastic $\mathbf{T}_{\mathrm{el}}=\frac{\delta W_{\mathrm{F}}}{\delta \hat{\mathbf{n}}}\times\hat{\mathbf{n}}$, viscous $\mathbf{T}_{\mathrm{vis}}=\frac{\delta \mathcal{R}^{\mathrm{vis}}}{\delta \hat{\mathbf{n}}_\tau}\times\hat{\mathbf{n}}$, and thermomechanical $\mathbf{T}_{\mathrm{tm}}=\frac{\delta \mathcal{R}^{\mathrm{tm}}}{\delta \hat{\mathbf{n}}_\tau}\times\hat{\mathbf{n}}$ torques, where $W_{\mathrm{F}}=\frac{1}{2}[(\nabla\cdot\hat{\mathbf{n}})^2+\frac{K_3}{K_1}(\hat{\mathbf{n}}\times\nabla\times\hat{\mathbf{n}})^2]$ is the dimensionless elastic energy, $\hat{\mathbf{n}}_\tau\equiv\frac{d\hat{\mathbf{n}}}{d\tau}$ is the material derivative of $\hat{\mathbf{n}}$, whereas

$$
\begin{aligned}
2\gamma_1\mathcal{R}^{\mathrm{vis}} &= \alpha_1(\hat{\mathbf{n}}\cdot\mathbf{D}_{\mathrm{s}}\cdot\hat{\mathbf{n}})^2+\gamma_1(\hat{\mathbf{n}}_\tau-\mathbf{D}_{\mathrm{a}}\cdot\hat{\mathbf{n}})^2\\
&+2\gamma_2(\hat{\mathbf{n}}_\tau-\mathbf{D}_{\mathrm{a}}\cdot\hat{\mathbf{n}})\cdot[\mathbf{D}_{\mathrm{s}}\cdot\hat{\mathbf{n}}-(\hat{\mathbf{n}}\cdot\mathbf{D}_{\mathrm{s}}\cdot\hat{\mathbf{n}})\hat{\mathbf{n}}]\\
&+\alpha_4\mathbf{D}_{\mathrm{s}}:\mathbf{D}_{\mathrm{s}}+(\alpha_5+\alpha_6)(\hat{\mathbf{n}}\cdot\mathbf{D}_{\mathrm{s}}\cdot\mathbf{D}_{\mathrm{s}}\cdot\hat{\mathbf{n}})^2
\end{aligned}
$$

is the viscous, and

$$
\begin{aligned}
\delta_1\mathcal{R}^{\mathrm{tm}} &= (\hat{\mathbf{n}}\cdot\nabla\chi)\mathbf{D}_{\mathrm{s}}:\mathbf{M}+\nabla\chi\cdot\mathbf{D}_{\mathrm{s}}\cdot\mathbf{M}\cdot\hat{\mathbf{n}}+(\hat{\mathbf{n}}\cdot\nabla\chi)[\hat{\mathbf{n}}_\tau\\
&-\mathbf{D}_{\mathrm{a}}\cdot\hat{\mathbf{n}}-3\mathbf{D}_{\mathrm{s}}\cdot\hat{\mathbf{n}}+3(\hat{\mathbf{n}}\cdot\mathbf{D}_{\mathrm{s}}\cdot\hat{\mathbf{n}})\hat{\mathbf{n}}]\cdot\mathbf{M}\cdot\hat{\mathbf{n}}\\
&+\hat{\mathbf{n}}(\nabla\mathbf{v})^{\mathrm{T}}\cdot\mathbf{M}\cdot\nabla\chi+\tfrac{1}{2}(\hat{\mathbf{n}}\cdot\mathbf{D}_{\mathrm{s}}\cdot\hat{\mathbf{n}})\,\nabla\chi\cdot\mathbf{M}\cdot\hat{\mathbf{n}}\\
&+\hat{\mathbf{n}}_\tau\cdot\mathbf{M}\cdot\nabla\chi+\tfrac{1}{2}\mathcal{M}_0\,\nabla\chi\cdot\nabla\mathbf{v}\cdot\hat{\mathbf{n}}\\
&+(\hat{\mathbf{n}}\cdot\nabla\chi)\mathcal{M}_0(\hat{\mathbf{n}}\cdot\mathbf{D}_{\mathrm{s}}\cdot\hat{\mathbf{n}})+\tfrac{1}{2}\mathcal{M}_0\hat{\mathbf{n}}_\tau\cdot\nabla\chi
\end{aligned}
$$

is the thermomechanical contributions to the full dimensionless Rayleigh dissipation function, respectively. Here $\mathbf{D}_{\mathrm{s}}=\frac{1}{2}[\nabla\mathbf{v}+(\nabla\mathbf{v})^{\mathrm{T}}]$ and $\mathbf{D}_{\mathrm{a}}=\frac{1}{2}[\nabla\mathbf{v}-(\nabla\mathbf{v})^{\mathrm{T}}]$ are the symmetric and asymmetric contributions to the rate of strain tensor $\mathbf{M}=\frac{1}{2}[\nabla\hat{\mathbf{n}}+(\nabla\hat{\mathbf{n}})^{\mathrm{T}}]$, and $\mathcal{M}_0=\nabla\cdot\hat{\mathbf{n}}$ is the scalar invariant of the tensor $\mathbf{M}$. We use here the invariant, multiple dot convention $\mathbf{ab}=a_ib_j$, $\mathbf{a}\cdot\mathbf{b}=a_ib_i$, $\mathbf{A}\cdot\mathbf{B}=A_{ik}B_{kj}$, and $\mathbf{A}:\mathbf{B}=A_{ik}B_{ki}$, where repeated Cartesian indices are summed.

The dimensionless ST σ_{ij} can be obtained directly from the elastic contribution to the energy and Rayleigh dissipation function as $\sigma^{\mathrm{el}}=-\frac{\partial W_{\mathrm{F}}}{\partial\nabla\hat{\mathbf{n}}}\cdot(\nabla\hat{\mathbf{n}})^{\mathrm{T}}$, $\sigma^{\mathrm{vis}}=\frac{\delta\mathcal{R}^{\mathrm{vis}}}{\delta\nabla\mathbf{v}}$, and $\sigma^{\mathrm{tm}}=\frac{\delta\mathcal{R}^{\mathrm{tm}}}{\delta\nabla\mathbf{v}}$, for the elastic, viscous, and thermomechanical contributions, respectively.

Straightforward calculations give the following expressions for ST components $\sigma_{ij}^{\mathrm{el}}$, $\sigma_{ij}^{\mathrm{vis}}$, and $\sigma_{ij}^{\mathrm{tm}}$ and functions $\mathcal{B}_{\mathrm{el}}$, $\mathcal{B}_{\mathrm{vis}}$, $\mathcal{B}_{\mathrm{tm}}$, and $\mathcal{D}_i(i=1,2,3)$ needed in Eqs. (5) and (6):

$$
\mathcal{B}_{\mathrm{el}}=n_z\mathcal{M}_{0,x}-n_x\mathcal{M}_{0,z}+\frac{K_3}{K_1}(n_zh_{,z}-n_xh_{,x}),
$$

$$
\begin{aligned}
\mathcal{B}_{\mathrm{vis}} &= n_x\frac{dn_z}{d\tau}-n_z\frac{dn_x}{d\tau}+\tfrac{1}{2}(w_{,x}-u_{,z})+n_xn_z(w_{,z}-u_{,x})\gamma\\
&+\gamma(n_x^2-n_z^2)(u_{,z}+w_{,x}),
\end{aligned}
$$

$$
\begin{aligned}
\mathcal{B}_{\mathrm{tm}} &= \chi_{,x}[-\tfrac{1}{2}n_z\mathcal{M}_0-n_zM_{xx}+n_x^2(n_xM_{zz}-M_{xx}n_z+2n_xM_{xz})]\\
&+\chi_{,z}[\tfrac{1}{2}n_x\mathcal{M}_0+n_xM_{zz}+n_z^2(n_xM_{zz}-M_{xx}n_x\\
&-2n_zM_{xz})],\quad \text{where}\quad h=n_{z,x}-n_{x,z}.
\end{aligned}
$$

The viscous components of the ST are

$$
\sigma_{xx}^{\mathrm{vis}}=g_1u_{,x}+n_xn_zg_2(u_{,z}+w_{,x})+\gamma(w_{,x}+n_x\frac{dn_x}{d\tau}),
$$

$$
\sigma_{zz}^{\mathrm{vis}}=-g_3w_{,z}+n_xn_zg_4(u_{,z}+w_{,x})+\gamma(-w_{,x}+n_z\frac{dn_z}{d\tau}),
$$

$$
\begin{aligned}
\sigma_{xz}^{\mathrm{vis}} &= -g_3w_{,z}+n_xn_zg_6(u_{,z}+w_{,x})+\tfrac{1}{2}(w_{,x}+n_z\frac{dn_x}{d\tau}-n_x\frac{dn_z}{d\tau})\\
&+\gamma(n_z\frac{dn_x}{d\tau}+n_x\frac{dn_z}{d\tau}),
\end{aligned}
$$

$$
\begin{aligned}
\sigma_{zx}^{\mathrm{vis}} &= g_3u_{,x}+n_xn_zg_7(u_{,z}+w_{,x})-\tfrac{1}{2}(w_{,x}+n_z\frac{dn_x}{d\tau}-n_x\frac{dn_z}{d\tau})\\
&+\gamma(n_z\frac{dn_x}{d\tau}+n_x\frac{dn_z}{d\tau}),
\end{aligned}
$$

with

$$
g_1=\tfrac{1}{\gamma_1}[\alpha_1n_x^2(n_x^2-n_z^2)+\alpha_4+(\alpha_5+\alpha_6)n_x^2],
$$

$$
g_2=\tfrac{1}{\gamma_1}(\alpha_1n_x^2+\tfrac{\alpha_5+\alpha_6}{4}-\tfrac{\gamma_2}{2}),
$$

$$
g_3=\tfrac{1}{\gamma_1}[\alpha_1n_z^2(n_x^2-n_z^2)-\alpha_4-(\alpha_5+\alpha_6)n_z^2],
$$

$$
g_4=\tfrac{1}{\gamma_1}(\alpha_1n_x^2+\tfrac{\alpha_5+\alpha_6}{4}+\tfrac{\gamma_2}{2}),
$$

$$
g_5=\tfrac{\alpha_1}{\gamma_1}n_xn_z(n_x^2-n_z^2),
$$

$$
g_6=\tfrac{1}{\gamma_1}[\alpha_1n_x^2n_z^2-\tfrac{\gamma_1}{4}+\tfrac{\gamma_2}{4}(n_z^2-n_x^2)+\tfrac{\alpha_4}{2}+\tfrac{\alpha_5+\alpha_6}{4}n_xn_z],
$$

$$
g_7=\tfrac{1}{\gamma_1}[\alpha_1n_x^2n_z^2+\tfrac{\gamma_1}{4}+\tfrac{\gamma_2}{4}(n_x^2-n_z^2)+\tfrac{\alpha_4}{2}+\tfrac{\alpha_5+\alpha_6}{4}n_xn_z].
$$

The elastic components of the ST are

$$
\sigma_{xx}^{\mathrm{el}}=-\mathcal{M}_0n_{x,x}-\frac{K_3}{K_1}hn_{z,x},\sigma_{zz}^{\mathrm{el}}=-\mathcal{M}_0n_{z,z}+\frac{K_3}{K_1}hn_{x,z},
$$

$$\sigma_{xz}^{\mathrm{el}} = -\mathcal{M}_0 n_{x,z} - \frac{K_3}{K_1} h n_{z,z}, \sigma_{zx}^{\mathrm{el}} = -\mathcal{M}_0 n_{z,x} + \frac{K_3}{K_1} h n_{x,x}.$$

The thermomechanical components of the ST are

$$\sigma_{xx}^{\mathrm{tm}} = \delta_1[\chi_{,x} h_1 + \chi_{,z} h_2], \quad \sigma_{zz}^{\mathrm{tm}} = \delta_1[\chi_{,x} h_3 + \chi_{,z} h_4],$$

$$\sigma_{zx}^{\mathrm{tm}} = \delta_1[\chi_{,x} h_5 + \chi_{,z} h_6], \quad \sigma_{xz}^{\mathrm{tm}} = \delta_1[\chi_{,x} h_7 + \chi_{,z} h_8],$$

where

$$h_1 = \tfrac{1}{2} n_x (M_{xx} + M_{zz}) + n_z M_{xz} + n_x^2 (-\tfrac{3}{2} n_x M_{xx} + n_x M_{zz} + \tfrac{1}{2} n_z M_{xz}),$$

$$h_2 = n_z M_{xx} - 2 n_x M_{xz} + n_x^2 (-2 n_z M_{xx} + \tfrac{3}{2} n_z M_{zz} + \tfrac{7}{2} n_x M_{xz}),$$

$$h_3 = \tfrac{3}{2} n_x M_{xx} - n_x M_{zz} + \tfrac{3}{2} n_z M_{xz} + n_x^2 (-\tfrac{3}{2} n_x M_{xx} + 2 n_x M_{zz} - \tfrac{7}{2} n_z M_{xz}),$$

$$h_4 = \tfrac{3}{2} n_z M_{xx} + 2 n_z M_{zz} - \tfrac{3}{2} n_x M_{xz} + n_x^2 (-n_z M_{xx} + \tfrac{3}{2} n_z M_{zz} + \tfrac{5}{2} n_x M_{xz}),$$

$$h_5 = 2 n_z M_{zz} + 4 n_x M_{xz} + n_x^2 (n_z M_{xx} - \tfrac{3}{2} n_z M_{zz} - \tfrac{5}{2} n_x M_{xz}),$$

$$h_6 = \tfrac{5}{2} n_x M_{zz} - \tfrac{1}{2} n_z M_{xz} + n_x^2 (\tfrac{3}{2} n_x M_{xx} - n_x M_{zz} + \tfrac{5}{2} n_z M_{xz}),$$

$$h_7 = \tfrac{3}{2} n_z (M_{xx} + M_{zz}) + 2 n_x M_{xz} + n_x^2 (n_z M_{xx} - \tfrac{3}{2} n_z M_{zz} - \tfrac{5}{2} n_x M_{xz}),$$

$$h_8 = \tfrac{1}{2} n_x (M_{xx} + 2 M_{zz}) + \tfrac{3}{2} n_z M_{xz} + n_x^2 (\tfrac{3}{2} n_x M_{xx} - n_x M_{zz} + \tfrac{5}{2} n_z M_{xz}).$$

The functions $\mathcal{D}_i (i=1,2,3)$ needed in Eqs. (6) are $\mathcal{D}_1 = \lambda n_x^2 + n_z^2$, $\mathcal{D}_2 = \lambda n_z^2 + n_x^2$, and $\mathcal{D}_3 = (\lambda - 1) n_x n_z$. Here, $\lambda = \lambda_{\parallel} / \lambda_{\perp}$.

The coefficients $\mathcal{B}_{ij} (i=1,2; j=1,\ldots,6)$ are

$$\mathcal{B}_{11} = g_1 + \tfrac{1}{2} - n_x n_z g_7, \quad \mathcal{B}_{12} = n_x n_z g_7, \quad \mathcal{B}_{13} = g_5 + n_x n_z g_2,$$

$$\mathcal{B}_{14} = n_x n_z g_2 + \gamma, \quad \mathcal{B}_{15} = g_{1,x} + g_{5,z},$$

$$\mathcal{B}_{16} = (n_x n_z g_2)_{,x} + (n_x n_z g_7)_{,z}, \quad \mathcal{B}_{21} = \tfrac{1}{2} + n_x n_z g_6,$$

$$\mathcal{B}_{22} = -g_3 - n_x n_z g_6, \quad \mathcal{B}_{23} = n_x n_z g_4 - \gamma - g_5,$$

$$\mathcal{B}_{24} = n_x n_z g_4, \quad \mathcal{B}_{25} = -g_{5,x} - g_{3,z},$$

$$\mathcal{B}_{26} = (n_x n_z g_4)_{,z} + (n_x n_z g_6)_{,x},$$

and the functions $\mathcal{F}_i (i=1,2)$ are

$$\mathcal{F}_1 = h_1 \chi_{,xx} + h_6 \chi_{,zz} + (h_2 + h_5) \chi_{,xz} + (h_{1,x} + h_{5,z}) \chi_{,x} + (h_{2,x} + h_{6,z}) \chi_{,z},$$

$$\mathcal{F}_2 = h_7 \chi_{,xx} + h_4 \chi_{,zz} + (h_3 + h_8) \chi_{,xz} + (h_{7,x} + h_{3,z}) \chi_{,x} + (h_{8,x} + h_{4,z}) \chi_{,z}.$$

[1] D. K. Yang and S. T. Wu, *Fundamentals of Liquid Crystal Devices* (John Wiley, New York, 2006).
[2] P. G. de Gennes and J. Prost, *The Physics of Liquid Crystals*, 2nd ed. (Oxford University Press, Oxford, 1995).
[3] R. S. Akopyan and B. Ya. Zeldovich, Sov. Phys. JETP **60**, 953 (1984).
[4] H. R. Brand and H. Pleiner, Phys. Rev. A **37**, 2736 (1988).
[5] A. V. Zakharov and A. A. Vakulenko, J. Chem. Phys. **127**, 084907 (2007).
[6] A. Dequidt and P. Oswald, EPL **80**, 26001 (2007).
[7] A. V. Zakharov, A. A. Vakulenko, and S. Romano, J. Chem. Phys. **128**, 074905 (2008).
[8] A. V. Zakharov and A. A. Vakulenko, Phys. Rev. E **79**, 011708 (2009).
[9] J. L. Ericksen, Arch. Ration. Mech. Anal. **4**, 231 (1960).
[10] F. M. Leslie, Arch. Ration. Mech. Anal. **28**, 265 (1968).
[11] L. D. Landau and E. M. Lifshitz, *Fluid Mechanics* (Pergamon, Oxford, 1987).
[12] I. W. Stewart, *The Static and Dynamic Continuum Theory of Liquid Crystals* (Taylor and Francis, London, 2004).
[13] P. Semenza, Nat. Photonics **1**, 267 (2007).
[14] M. L. Cordero, E. Verneuil, F. Gallaire, and Ch. N. Baroud, Phys. Rev. E **79**, 011201 (2009).
[15] I. S. Berezin and N. P. Zhidkov, *Computing Methods*, 4th ed. (Pergamon Press, Oxford, 1965).